Performance Evaluation of Network-Admissible Demand Dispatch in Multi-Phase Distribution Grids

Mohammad Asif Iqbal Khan and Sumit Paudyal
Department of Electrical and Computer Engineering
Florida International University
Miami, USA
{mkhan103, spaudyal}@fiu.edu

Mads Almassalkhi
Department of Electrical and Biomedical Engineering
University of Vermont
Burlington, USA
malmassa@uvm.edu

***Abstract*—As the penetration of flexible loads increases in distribution networks, demand dispatch schemes need to consider the effects of large-scale load control on distribution grid reliability. More specifically, we need demand dispatch schemes that actively ensure that distribution grid operational constraints are not violated (i.e., network-admissible) and still deliver valuable market services. For network-admissible demand dispatch schemes that depend on live 3-phase grid measurements, their overall performance and ability to manage constraints depends on the number, update rate, and multi-phase nature of the available measurements. In this context, the manuscript develops and evaluates the performance of a new network-admissible version of the device-driven demand dispatch scheme called Packetized Energy Management (PEM) within a large multi-phase distribution feeder. Specifically, this work investigates the effects of different levels and rates of grid measurements for a practical-sized, 2,522-node, unbalanced distribution test feeder with 3000 flexible kW-scale loads operating under the network-admissible PEM scheme. The results demonstrate the value of live grid measurements in managing distribution grid operational constraints while PEM is able to effectively deliver frequency regulation services.**

***Index Terms*—Demand dispatch, distribution grid, load management, distributed energy resources, voltage control.**

I. Introduction

The number, density, and diversity of behind-the-meter (BTM) distributed energy resources (DERs) and loads, such as thermostatically-controlled loads (TCLs), deferrable loads, and battery storage systems (BSS) are increasing in today's distribution systems. Via demand dispatch approaches, these connected DERs can be aggregated to provide different energy services at the bulk power level, while ensuring quality of service (QoS) for end users [1]–[4]. However, existing demand dispatch schemes often focus on coordinating devices and managing end-user device constraints and overlook the distribution grid's operational constraints. To incorporate both end-user QoS and grid constraints, one could naively construct a large (NP-hard) grid-aware device scheduling problem that embeds the distribution grid optimal power flow (OPF) problem and whose solution represents an optimal device dispatch. However, such approach generally scales poorly with the number of controllable end-points and the non-convex AC power flow constraints of large distribution networks. Furthermore, such OPF-based demand dispatch methods, which can enforce grid constraints and customers' QoS, rely on accurate and idealized network parameters and load/renewable generation forecasts, and are typically solved at minutes to sub-hourly intervals, which may not sufficiently capture the high variability on system conditions (e.g., rapid voltage fluctuations) caused by the DERs nor fast market conditions (e.g., frequency regulation) [5].

Ensuring grid feasibility is crucial for any demand-side management (DSM) activities. In this context, the authors in [6] proposed congestion and voltage profile management by estimating the expected network profiles (voltage, power flow, etc.) and energy usage variations. To ensure grid feasibility of diverse DERs, the work in [7] uses multi-period optimization models to aggregate the active power flexibility by approximating the exact feasible region of the net power injection at the substation level with an inner-box region. In [8], authors propose node-wise computation of power injection and withdrawal limits using OPF-based models. Disaggregating the net flexibility as obtained in [7] to nodal level or estimating the nodal injection bounds that ensures grid feasibility could still render challenging optimization problems [4], [9]. Therefore, in [10], [11], the authors developed a provable convex inner approximation of the feasible region that is able to disaggregate dispatch signals to nodal level that do not violate the grid constraints. Realising the uncertainty of incoming usage request of connected flexible loads, in [12] the authors developed a control formulation for handling plug-and-play charging requests of flexible loads in a distribution system and ensured grid feasibility through a convex formulation of the distribution grid model [13]. The grid feasibility can also be ensured through the estimation of DER and flexible load hosting capacity as in [14], [15]. In [16], [17], the grid feasibility is ensured through the design of local droop settings to control active/reactive power of DERs.

Given the high computational needs, the optimization based models are intended to provide bounds at coarse time scale (sub-hourly) that may not capture high variability on grid conditions due to intermittency of DERs. To ensure robustness in managing the grid constraints, particularly for forecasting uncertainties and high variabilities of DERs, the coarse time-step, optimization-based methods can be complemented by feedback obtained from the grid measurements/state estimators [18], [19]. That is, as the deployment of low-cost sensors at the grid-edge intensifies and are combined with existing real-time automatic controllers (RTAC) and micro-phasor measurement units (μ-PMU), it opens up new data-driven applications for feedback-based coordination of DERs in power distribution networks that respects constraints and network limits [20].

In this paper, we incorporate grid measurements (or es-

This work was supported by the U.S. Department of Energy's Advanced Research Projects Agency—Energy (ARPA-E) Award DE-AR0000694. M. Almassalkhi is co-founder of startup Packetized Energy, which seeks to bring to market a commercially viable version of Packetized Energy Management.

timates) with a recently-developed, bottom-up coordination scheme called packetized energy management (PEM), please see [21]. The combination of sensor measurements and coordination begets a novel grid-aware implementation of PEM. Unlike many other grid-aware coordination methods, the presented approach leverages the device-driven nature of PEM and employs 'traffic-light logic' with grid measurements and constraint violations to make real-time and local decisions about devices. At its core, PEM employs internet-like packet protocols to coordinate the energy consumption of TCLs by having each device asynchronously and probabilistically request a finite-duration, fixed-power energy packet based on its local need for energy (e.g., temperature within its deadband or its state of charge). The PEM coordinator then accepts or denies individual energy packet requests to regulate the aggregate load based on a desired reference. If the coordinator accepts more packet requests than packets that expire, then the aggregate demand increases. Otherwise, it decreases. However, to ensure that devices can meet local energy requirements, PEM also enables devices whose energy packet requests have been denied to temporarily opt-out of the scheme and consume energy, if it needs to do so to preserve the end-user's QoS. The opted out device returns to PEM once QoS has been restored (e.g., the temperature or SoC is returned strictly within deadband). Thus, we term PEM to be QoS-aware.

PEM has been developed recently and analyzed in a variety of settings. For example, PEM was initially developed for electric water heaters and demonstrated a peak demand curtailment scenario [22], extended to consider bidirectional energy storage devices and diverse groups of DERs while providing synthetic balancing reserves [21], modeling and control of DERs [23]–[25], and characterization of demand flexibility under PEM [26], [27]. Recent work shows how the packet duration (or packet length) in PEM determines the speed of the closed-loop response and the type of grid-services PEM can provide. In particular, to effectively deliver frequency regulation, shorter packets lengths of 1-3 minutes are needed, but leads to more device on-off cycling (i.e., increased wear-and-tear) [28]. The probability-to-request in PEM determines the average number of request at the coordinator within a short time period, which represents that ability of the fleet to ramp up or down (depending on request types) and is related to the fleet's flexible capacity. This analysis has lead to the notion of randomized packet lengths, which have been shown to both improve the speed of response and reduce device cycling [28]. However, prior work on PEM has focused exclusively on grid-agnostic coordinator that effectively ignores the underlying distribution networks. As the density of devices increase in the medium/low-voltage networks, incorporating grid conditions and measurements will become important. Therefore, we extended PEM by developing a 'Network-Admissible PEM', in which the grid operational constraints are respected in real time while delivering ancillary market services in the aggregate (and preserving end-user's QoS).

However, like in any measurement-based closed-loop voltage control of distribution feeders, the performance of 'Network-Admissible PEM' depends on the number of available measurements, frequency of the measurement update, and multi-phase measurement considerations. Note that placing sensors (e.g., μ-PMUs) on every node on the distribution circuits, and updating the measurements frequently incur high infrastructure costs and require extensive communication networks and bandwidth. Critically, this may not be necessary due to overall improvements in managing system-level constraints with a few additional grid measurements. Moreover, most of the works on voltage control with behind-the-meter assets focus on single-phase or phase decoupled circuits. Removal of mutual impedance from distribution circuits causes significant voltage error in the phase-decoupled models [29]. Specifically, the intra-phase dependency is not straightforward as active voltage control in one phase can worsen the voltage profiles on other phases [30]; hence, it necessities full three-phase voltage measurements for effective control of unbalanced distribution feeders. In this context, this work contributes as following,

- It provides practically-relevant, simulation-based analysis on the effects of the number, type, and sampling rate of grid measurement updates on the overall performance of the Network-Admissible PEM.
- Unlike the local voltage control schemes common in phase-decoupled circuits, this work considers phase-coupled unbalanced distribution grids in the Network-Admissible PEM and demonstrates the significance of intra-phase measurements on the effective voltage control of multi-phase distribution grids.

II. Packetized energy management preliminaries

This section provides a summary of grid-agnostic PEM control logic at the device and coordinator layers.

A. Device Level PEM Logic

Consider device n with measured or estimated energy state over discrete time interval k of duration Δt, $x_n[k]$. This device is endowed with local control logic that relates the $x_n[k]$, its user-defined set-point x_n^{set}, and its comfort range, $[\underline{x}_n, \overline{x}_n]$, to a probability of making a request for a finite-duration, fixed-power energy packet to the coordinator (e.g., 5-minute, 4 kW or 0.33 kWh energy packet request). As an example, the probability that device n makes a request during interval Δt is illustrated in Fig. 1 via the following relation for a charging (i.e., power consumption) packet:

$$P_{\text{req}}(k) := 1 - e^{-m_R \mu_n(x_n[k])\Delta t} \tag{1}$$

where m_R is the mean time-to-request (MTTR) when $x_n[k] = x_n^{\text{set}}$ and $\mu_n(x_n[k]) \geq 0$ is a state-dependent rate parameter given by,

$$\mu_n(x_n[k]) := \begin{cases} \frac{\overline{x}_n - x_n[k]}{x_n[k] - \underline{x}_n} \cdot \frac{x_n^{\text{set}} - \underline{x}_n}{\overline{x}_n - x_n^{\text{set}}} & \text{if } x_n[k] \in (\underline{x}_n, \overline{x}_n) \\ 0 & \text{if } x_n[k] \geq \overline{x}_n \end{cases}. \tag{2}$$

Discharging (i.e., power injection) packet request logic can be defined similarly and is also illustrated in Fig. 1. Thus, for a given local dynamic energy state (or a device's need for energy), the probability of making a request is defined. This probability is compared with an independent sample from uniform distribution to determine if a request is made from device n at time-step k.

If the request is made and accepted by the coordinator, the device switches from standby to a constant-power

charging/discharging (consumes/supplies energy) state at the device's rated power level $\pm P_n^{\text{rate}}$. The constant power level is maintained for the duration of the packet length when the packet then *expires*, unless the packet is *interrupted* prematurely (to avoid exceeding the comfort range).

In addition, if a device's requests are repeatedly denied by the coordinator, the device's energy state may exceed its comfort range. Owing to the QoS-aware design of PEM, the device will then notify the coordinator that it is automatically *opting out* of PEM and will consume/supply the necessary energy to return the energy state to within its defined comfort range upon which the device updates the coordinator that it has returned to PEM mode. The use of packet-based (net) consumption and event-based device communications represents a novel, scalable approach for a centralized coordinator to estimate the aggregate demand without real-time power measurements from the entire fleet. Next, we define how packet requests are managed by the PEM coordinator to dynamically regulate aggregate (net) demand.

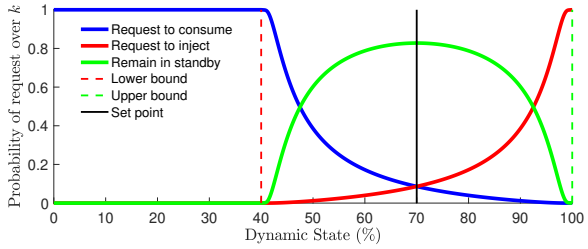

Fig. 1: Probability of a bidirectional device (e.g., ESS) requesting to the coordinator to either consume power (blue) or inject power (red) over a discrete-time interval k. If neither or both request types are made, then the device remains in standby (green). Clearly, for an electric water heater, there is no option to inject power, so device's packet request logic simplifies.

B. Coordinator Level PEM Logic

Due the asynchronous implementation of PEM, an energy packet request from any device can arrive at the coordinator at any time. This implies that over a sufficiently small time interval (e.g, 10ms, which can be different from device's interval Δt), it is reasonable to assume that the coordinator only receives a single device event. The event could be an incoming charging/discharging packet request, $u_{\text{c/d},n}[k] \in \{0,1\}$, which is either accepted or rejected (i.e., $y_{\text{c/d},n}[k] \in \{0,1\}$ with $y_{\text{c/d},n}[k] \leq u_{\text{c/d},n}[k]$). Besides packet requests, the coordinator can also receive event types related to previously accepted packets expiring ($y^{\text{exp}}_{\text{c/d},n}[k]=1$) or being interrupted ($y^{\text{int}}_{\text{c/d},n}[k]=1$) and devices opting out ($y^{\text{opt}}_{\text{c/d},n}[k]=1$). From the incoming stream of events, the coordinator can then construct an online estimate of the aggregate demand. For example, for a fleet of switch loads (i.e., with only charging packets and $P_n^{\text{rate}} > 0$), the aggregate demand at time-step k can be estimated as:

$$P_{\text{agg}}[k+1] := P_{\text{agg}}[k] + \sum_{n=1}^{N} P_n^{\text{rate}} \Delta y_{\text{c},n}[k], \qquad (3)$$

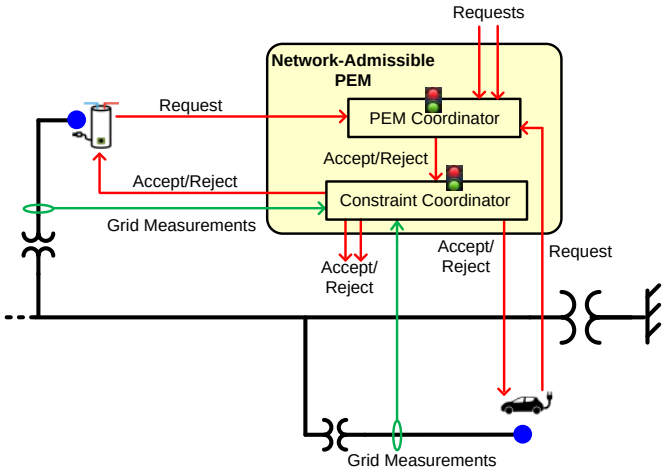

Fig. 2: Network-Admissible PEM-based demand dispatch scheme.

where, $\Delta y_{\text{c},n}[k] := y_{\text{c},n}[k] - y^{\text{exp}}_{\text{c},n}[k] - y^{\text{int}}_{\text{c},n}[k] + y^{\text{opt}}_{\text{c},n}[k]$ and we assume that the time-step k is sufficiently small such that no more than a single device event takes place across the fleet (i.e., $\sum_{n=1}^{N} y_{\text{c},n}[k] + y^{\text{exp}}_{\text{c},n}[k] + y^{\text{int}}_{\text{c},n}[k] + y^{\text{opt}}_{\text{c},n}[k] \leq 1$ for all k). Clearly, the aggregate demand increases when packets are accepted or devices opt out and demand decreases when a packet expires or is interrupted. Note that the coordinator's only decision is whether to accept or reject a packet request (i.e., determine $y_{\text{c/d},n}[k]$), which is based on the difference between $P_{\text{agg}}[k]$ and a desired target reference power $P_{\text{ref}}[k]$.

This gives rise to the coordinator's control policy, whose objective is to minimize the tracking error $e[k] := P_{\text{ref}}[k] - P_{\text{agg}}[k]$ and is defined as follows for a fleet of switch loads:

$$y_{\text{c},n}[k] := \begin{cases} 1, & \text{if } u_{\text{c},n}[k]=1 \ \wedge \ e[k] \geq P_n^{\text{rate}}/2 \\ 0, & \text{else} \end{cases}. \qquad (4)$$

Generalizing the above to the case of coordinating a fleet with both charging and discharging requests is straightforward. For further details on modeling and control of a fleet under PEM, please see prior works [21], [24], [25], [28]. Note that the coordinator's control policy is similar to a relay controller that accepts a packet when the tracking error is above a threshold ("green light") and reject otherwise ("red light"). However, unlike traditional relay control from a single plant, the coordinator responds to asynchronous, stochastic requests from N plants, which permits accurate tracking.

The key contribution in this manuscript is to extend the coordinator's control policy in (4) to incorporate and understand the effect of distribution grid measurements into the packet acceptance/rejection logic. These measurements enable PEM to be cognizant of the network's nodal voltage and transformer apparent power limits and only accept packet request if they reduce tracking error **and** do not exacerbate any network violations, which gives rise to a *Network-Admissible PEM* and is described next.

III. Network-Admissible PEM

A. Overall Approach

The overall Network-Admissible PEM approach is illustrated in Fig. 2, where the PEM coordinator as in [21], [22]

is integrated with a (grid) Constraint Coordinator. In regular PEM scheme, energy packet requests are made by the devices to the PEM coordinator, which are accepted or rejected by the coordinator in real time to track desired reference setpoints (as explained in Section II). The accepted requests are handled by the Constraint Coordinator in the next step, which checks the grid constraints based on live grid measurements to generate traffic-like logic to determine, in real time, whether packets requests are network admissible.

B. Network-Admissible PEM Algorithm

Consider i_p represents index for a single phase node at bus i, i_{p+} represents all the phases of the same bus where node i is connected to, and $M[i_p] \in \{0,1\}$ is a parameter that represents if voltage at node i_p is measured or not. $\underline{V[i_p]}$ and $\overline{V[i_p]}$ are the prescribed minimum and maximum voltage magnitude bounds. Based on the overall approach shown in Fig. 2 and the multi-phase voltage measurement consideration as described earlier, we build the proposed Network-Admissible PEM algorithm as shown in Algorithm 1. Note that Algorithm 1 is provided with respect to charging packet requests only under multi-phase measurement consideration (as represented by i_{p+}); however, similar logic can be readily developed for discharging packet request, single phase representation and varying constraint set in the Network-Admissible PEM.

Algorithm 1 : Network-Admissible PEM

1: Incoming Packet Request $u_{c,n}[k]$
2: **if** $\neg(u_{c,n}[k] = 1 \ \wedge \ e[k] \geq P_n^{\text{rate}}/2)$ **then** ▷ Refer to (4).
3: Reject Packet: $y_{c,n}[k]$=0.
4: **else** ▷ Grid Constraint Management.
5: **if** $M[i_p] = 1$ **then** ▷ Node i_p is measured.
6: **if** $\underline{V[i_{p+}]} \leq \left|V[i_{p+},k]\right| \leq \overline{V[i_{p+}]}$ **then**
7: Accept Packet: $y_{c,n}[k]$=1.
8: **else** ▷ Voltage violation.
9: Reject Packet: $y_{c,n}[k]$=0.
10: **end if**
11: **else**
12: Accept Packet: $y_{c,n}[k]$=1.
13: **end if**
14: **end if**

Upon receiving a packet request, $u_{c,n}[k]$, and passing line 2 of Algorithm 1 into line 4, the packet request enters 'Grid Constraint Management' part of the algorithm. At this point, the device requesting a packet appends its nodal ID to the request, i_p. The coordinator checks to see if it has access to the measurement i.e., if $M[i_p] = 1$, multi-phase voltage magnitude, $|V[i_{p+}]|$, at that node. The coordinator then accepts the packet request, only if doing so does not lead voltages to exceed their limits or exacerbate voltage violation.

IV. Numerical Simulation

In this section, we study the impact of varying PEM packet length (P_t) and grid voltage measurement update rate (S_t) on the Network-Admissible PEM scheme. We also evaluate the performance of Network-Admissible PEM scheme with single-phase versus multi-phase voltage measurements. Additionally, we study the impact of the number of voltage measurements on the performance of Network-Admissible PEM scheme.

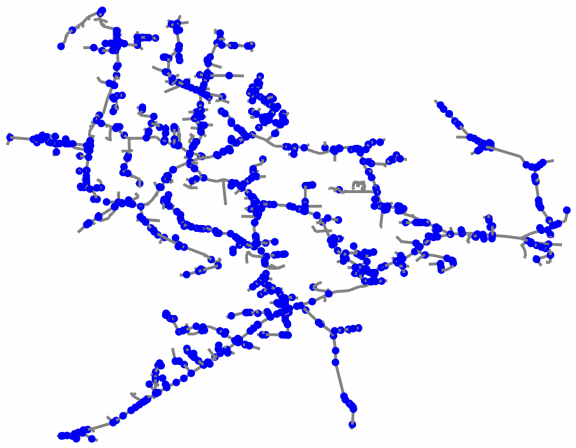

Fig. 3: A 2522-bus test feeder, modified from the original IEEE 8,500-node feeder, with 3,000 TCL and ESS devices.

A. Simulation Setup

A 2522-bus (3,817 single-phase nodes) test system as shown in Fig. 3, which is extracted from MV-side of the IEEE 8500-node test feeder [31], is used for numerical case studies. The test system shown in Fig. 3 has a total of 1,413 single-phase load nodes, where TCLs and ESSs devices are connected and are controlled through Network-Admissible PEM scheme. Total of 3,000 PEM controlled devices (2,100 TCLs and 900 ESS) are connected to the load nodes. Each load has up to three PEM devices (TCL or ESS), and each device has $P_n^{\text{rate}} = \pm 5$kW. Different packet lengths are used in the simulation and MTTR is kept same as the packet length. The simulations are run for 1 hour with time step of 2 seconds (i.e., 1,800 time steps). The load data in the IEEE feeder is modified and a total PV of 7 MW are connected to the the existing load at 200 nodes (among 1,413 load nodes) to create over-voltage scenario. Fig. 4 shows base load and the net load modified with injection of PV and the impact on the maximum voltage magnitude across the network for the entire simulation period of 1 hour.

B. Performance Metrics

We adopt the following metrics to evaluate the performance of the Network-Admissible PEM.

Composite Performance Score (x_c): This score is used in industry by system operator PJM and measures the overall performance of a grid resource to regulate to the AGC reference signal. The performance score is the average of three distinct scores namely, accuracy, delay, and precision scores. For details on scores, please see [28].

Voltage Violation Metrics: At the system level, we propose to use the following three voltage violation metrics.

- **Maximum Duration of Continuous Voltage Violation** (D_m): This metric looks at any node on distribution feeder that exhibits the longest duration of voltage violation, i.e., $\left|V[i_p,k]\right| \geq \overline{V[i_p]} \vee \left|V[i_p,k]\right| \leq \underline{V[i_p]}$.

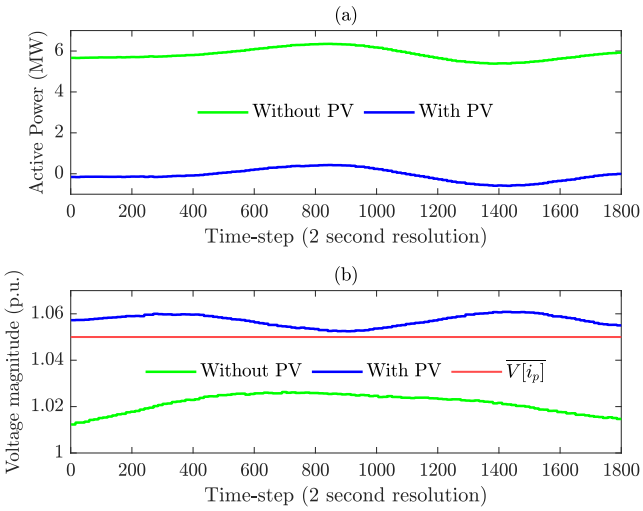

Fig. 4: Impact of PV : a) Modification of base-load profile and b) comparison of maximum of all nodes in presence and absence of PV.

- **Maximum Cumulative Duration of Voltage Violations** (D_t): Since there exists multiple instances of continuous voltage violation on distribution feeders, D_m alone is not sufficient to capture the temporal distribution of voltage violation. Thus, we propose to use D_t that is the maximum of the cumulative duration of nodal voltage violation.
- **Maximum Area under the Voltage Violation** (A_m): Metrics D_m and D_t defined above only capture the duration of voltage violation; however, these metrics are not able to capture the magnitude of voltage violations. Therefore, we propose to use maximum of cumulative area under the nodal voltage violation function (i.e., area under the voltages above or below the thresholds).

C. Performance Evaluation

The combined impact of varying packet lengths P_t and grid measurement update rate S_t on the performance metrics are analysed next. To obtain average performance metrics, each case is run 200 times that ensures randomness in the packet requests from TCLs and ESSs. Nodal voltage measurement update rate S_t is varied between 2 seconds, 30 seconds, 2 minutes, and 5 minutes for each of the packet length P_t of 30 seconds, 2 minutes, and 5 minutes.

Fig. 5 presents a sample case (one out of 200 runs) in tracking a real AGC signal with varying packet lengths with S_t =2 seconds. As we can see from the Figure, with the 30-second packet length the tracking performance is superior, which degrades gradually with 2-minute and 5-minute packet lengths. Fig. 6 shows another sample case in tracking AGC by varying measurement update rates (with $P_t = 5$ minutes). As we can see from the Figure, tracking starts deteriorating as S_t is increased gradually from 2 seconds to 5 minutes.

The impact of S_t on system-wide voltage performance is shown in Fig. 7 for the sample case of Fig. 6 with P_t= 5 minutes. The simulation comprises of 6,870,600 instances of

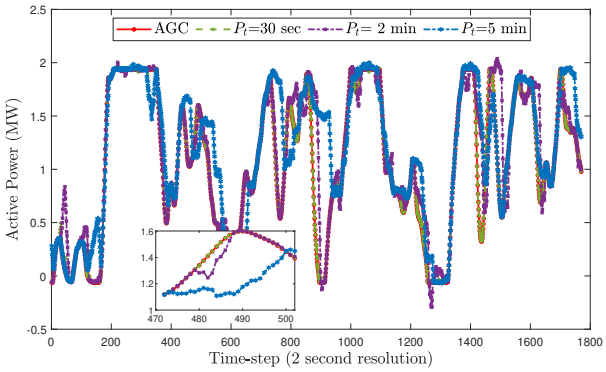

Fig. 5: Impact of packet length P_t on tracking performance of Network-Admissible PEM with $S_t = 2$ seconds.

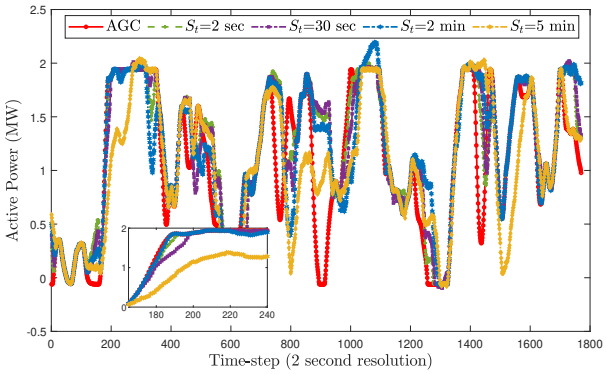

Fig. 6: Impact of measurement update rate S_t on tracking performance of Network-Admissible PEM with $P_t = 5$ minutes.

voltage that correspond to 1,800 time steps simulation (1 hour) of 3,817 single-phase nodes of the test feeder. For $S_t = 2$ seconds, 130 nodes (5,405 voltage instances) experienced voltage over 1.05 p.u. As S_t is increased to 30 seconds and 2 minutes, the overvoltage instances increased. With $S_t = 5$ minutes, the total nodes with overvoltage increased to 483 (with 62,584 voltage instances).

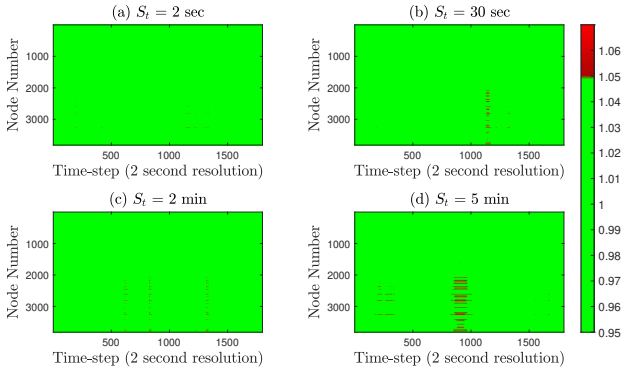

Fig. 7: System-wide voltage violation on the distribution feeder with varying level of measurement update rate S_t.

Fig. 8 (a) shows comparison of the maximum duration of continuous voltage violation (D_m), which is averaged over 200

runs for each value of P_t and S_t. For each packet length, as we increase S_t, the duration D_m increases. For example, with $P_t = 30$ seconds, D_m varies from 18 seconds to 240 seconds (out of 3,600 seconds of simulation) by varying S_t. With a coarse P_t (5 minutes), and measurement update rate of $S_t = 5$ minutes, D_m is 372 seconds, which is about 10% of total simulation duration and is significant overvoltage duration. We observed similar trend on maximum cumulative duration of voltage violation metric (D_t) (see Fig. 8 (b)) and the area under the voltage violation metric (A_m) (see Fig. 8 (c)). We observed from the case studies that both packet length (P_t) and measurement update rate (S_t) impact the voltage performance metrics considerably.

Fig. 8 (d) shows the composite score (x_c) in tracking the sample AGC signal. Value of x_c degrades as P_t and S_t are increased. However, the tracking performance is more dependent on the choice of P_t, and less impacted by S_t for a given value of P_t. Though it is preferred to use finer packet length for improved x_c, a packet length of $P_t = 2$ minutes in the Network-Admissible PEM schemes provided acceptable composite score and voltage performance metrics. This observation on composite score corroborates with the findings in previous work with PEM scheme (without grid constraints) [28]. Though x_c has acceptable value even with $P_t = 5$ minutes, this is not advisable from voltage performance point of view. However, if we compliment the coarse packet length with faster grid measurement update rate (e.g., $P_t = 5$ minutes and $S_t = 2$ seconds) we can achieve acceptable voltage performance. Similarly, if PEM uses fine packet length (e.g., $P_t = 30$ seconds), the grid measurements can be updated at slower rate for an acceptable voltage performance.

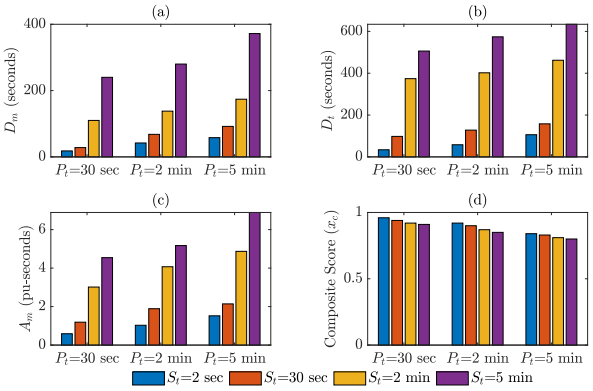

Fig. 8: Voltage violation metrics $(D_m,\ D_t,$ and $A_m)$ and composite performance score (x_c) for different values of packet length (P_t) and measurement update rate (S_t).

D. Impact of Number of Voltage Measurement Buses

The number of voltage measurement buses are changed from 0% (no measurements) to 100% (i.e., all buses with TCLs and ESSs) at a step of 20%. The impact of the number of measurement on the performance metrics is shown in Fig. 9 with $P_t = 5$ minutes and $S_t = 2$ seconds for varying number of measurement buses. With no voltage measurement (i.e., equivalent to regular PEM schemes as in [21], [22]), D_m is 374 seconds (out of 3,600 seconds of simulation), which is significant voltage violation, and reduces to 58 seconds (85% improvement) when the grid is fully measured (at TCL and ESS locations). We observed similar trend on D_t and A_m metrics.

The composite score x_c from AGC reference-tracking in Fig. 9(d) shows a very small decline as the number of grid measurements increase. However, the increasing penetration of nodal measurements leads to more potential for packet rejections due to strict grid conditions.

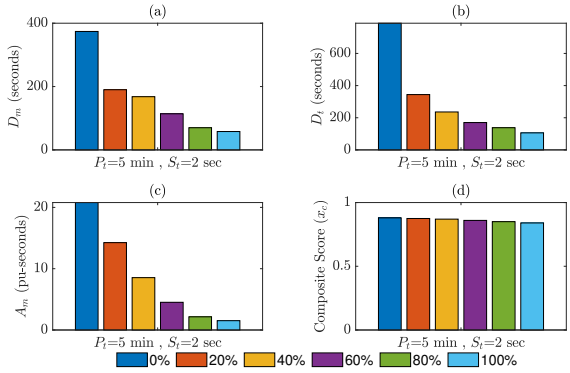

Fig. 9: Voltage violation metrics $(D_m,\ D_t,$ and $A_m)$ and composite performance score (x_c) for different number of voltage measurement buses.

E. Impact of Multi-Phase Measurements

This section evaluates the significance of intra-phase voltage measurements on the effective voltage control on single-phase nodes of multi-phase unbalanced feeders. To do so, we have simulated cases with voltage measurements obtained only from the node where PEM devices are connected and compared with multi-phase voltage measurement consideration.

As explained earlier, this test case has in total of 3,000 devices (mixed TCLs and ESSs) connected to multiple phases across the network. Though the simulations are carried out for various combinations of P_t and S_t, the following discussion is based on results with $P_t = 2$ minutes (short packets) and $S_t = 2$ seconds (frequent grid measurements). For this specific case, the total number of requests per time step from the devices ranges from a minimum of 19 to maximum of 87 devices. For the entire time duration of the simulation, a total of 70,742 requests are received and 454 requests are rejected due to multi-phase measurements.

Fig. 10 presents the voltage magnitude (in p.u.) of nodes 2593, 2594, and 2595, which are phases a, b, and c, respectively, of bus number 602 in the feeder. Out of these three phases, we are investigating the devices connected at node 2593 (phase a), where two PEM-enabled devices are connected ($P_n^{\text{rate}} = \pm 5$ kW). We can observe that the the voltage profile of phase a (where the device is connected) never exceeds the $\overline{V[i_p]}$ of 1.05 p.u.; however the phase c voltage shows significant instances of over-voltage. A closer look in Fig. 11 for time step between 1196 and 1300 seconds of simulation window shows the impact of the multi-phase measurement based control. Corresponding to the requests made at time-steps 1201, 1214 and 1225, which all are evaluated based on voltages on all phases to be under $\overline{V[i_p]}$, and hence the packet

requests are accepted. However, for the time steps 1266, 1270, 1278, 1287, and 1296, although the voltage at the device-connected node, i.e., at phase a (node 2593) is well under $\overline{V[i_p]}$, phase c is exhibiting voltage value over $\overline{V[i_p]}$, hence, the request is rejected. If multi-phase measurements were not used, then these requests would also be accepted.

The stricter control based on three-phase measurements leads to the performance metrics in Fig. 12, which shows the overall comparison of performance metrics with $P_t = 2$ minutes and $S_t = 2$ seconds for both single-phase and multi-phase measurements. Fig. 12 shows that all voltage violation metrics are significantly improved when multi-phase measurements are considered. However, as discussed in the previous case in Section IV-D, the voltage measurement did not considerably impact the composite score x_c in tracking the reference AGC signal here as well. This case study clearly shows that the single-phase measurement-based local voltage control approach as in [32] is not effective in managing voltages in three-phase unbalanced systems due to the phase coupling effect, whereas intra-phase measurements can ensure better voltage performance in multi-phase distribution feeders.

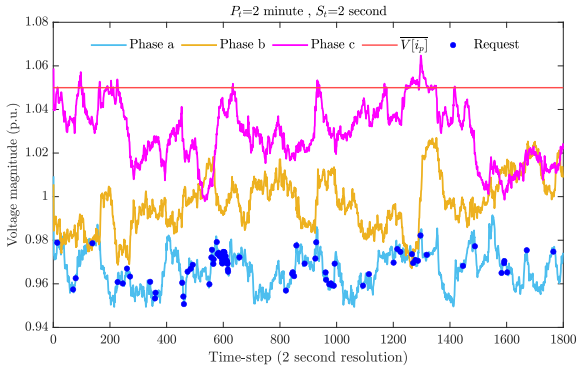

Fig. 10: Incoming requests from Phase a connected devices and the voltage profile of all phases.

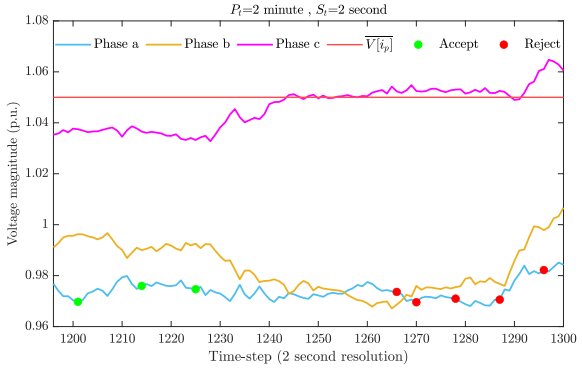

Fig. 11: Impact of multi-phase measurement in decision making against incoming requests.

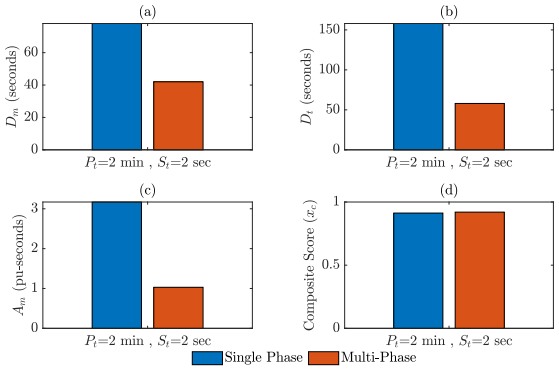

Fig. 12: Voltage violation metrics (D_m, D_t, and A_m) and composite performance score (x_c) for single-phase vs. multi-phase voltage measurements.

V. Conclusion

This paper provides comprehensive performance evaluation of a Network-Admissible demand dispatch algorithm in maintaining grid voltages and tracking reference (e.g., AGC signals). The Network-Admissible demand dispatch represents a generalization of PEM scheme by incorporating a new grid constraint management algorithm. This work demonstrated the impact of packet length (in PEM), grid voltage measurement update rate, the number of voltage measurement buses, and multi-phase measurements in managing the grid voltages and in tracking the power reference signal. Based on the simulation-based analysis carried out in a 2522-bus three-phase unbalanced distribution feeder, we observed that a) the tracking performance is less dependent on grid measurements and is more dependent on the packet length, b) voltage performance depends on both grid measurements and packet length, c) coarse packet length if complemented by fast grid measurement update rate can provide acceptable voltage performance, and d) multi-phase measurements are essential for effective voltage control of multi-phase distribution feeders. Future work will leverage OPF-based methods to derive time-varying nodal supply/demand capacity limits, which can reduce the number of measurements required.

References

[1] D. S. Callaway and I. A. Hiskens, "Achieving controllability of electric loads," *Proceedings of the IEEE*, vol. 99, no. 1, pp. 184–199, 2010.

[2] S. Rahman, "Framework for a resilient and environment-friendly micro-grid with demand-side participation," in *Proc. IEEE Power and Energy Society General Meeting - Conversion and Delivery of Electrical Energy in the 21st Century*, July 2008, pp. 1–1.

[3] F. B. dos Reis, K. Duwadi, R. Foutney, R. Tonkoski, T. M. Hansen, M. A. I. Khan, and S. Paudyal, "Impact of residential load models for overvoltage prevention studies in pv-rich lv grids," in *2019 IEEE Milan PowerTech*, 2019, pp. 1–6.

[4] J. Wang, E. Y. Ucer, S. Paudyal, M. C. Kisacikoglu, and M. A. I. Khan, "Distribution grid voltage support with four quadrant control of electric vehicle chargers," in *2019 IEEE Power Energy Society General Meeting (PESGM)*, 2019, pp. 1–5.

[5] D. S. Kirschen and G. Strbac, *Fundamentals of power system economics*. John Wiley & Sons, 2018.

[6] H. Liao and J. V. Milanovic, "Flexibility exchange strategy to facilitate congestion and voltage profile management in power networks," *IEEE Transactions on Smart Grid*, vol. 10, no. 5, pp. 4786–4794, Sep. 2019.

[7] X. Chen, E. Dall'Anese, C. Zhao, and N. Li, "Aggregate power flexibility in unbalanced distribution systems," *IEEE Transactions on Smart Grid*, vol. 11, no. 1, pp. 258–269, 2020.

[8] D. Molzahn and L. A. Roald, "Grid-aware versus grid-agnostic distribution system control: A method for certifying engineering constraint satisfaction," in *Proc. 52nd Hawaii International Conference on System Sciences*, 2019.

[9] J. Wang, G. R. Bharati, S. Paudyal, O. Ceylan, B. P. Bhattarai, and K. S. Myers, "Coordinated electric vehicle charging with reactive power support to distribution grids," *IEEE Transactions on Industrial Informatics*, vol. 15, no. 1, pp. 54–63, 2019.

[10] N. Nazir and M. Almassalkhi, "Convex inner approximation of the feeder hosting capacity limits on dispatchable demand," in *Proc. IEEE 58th Conference on Decision and Control (CDC)*, 2019, pp. 4858–4864.

[11] N. Nazir and M. Almassalkhi, "Grid-aware aggregation and realtime disaggregation of distributed energy resources in radial networks," *arXiv preprint arXiv:1907.06709*, 2019.

[12] C. Le Floch, S. Bansal, C. J. Tomlin, S. J. Moura, and M. N. Zeilinger, "Plug-and-play model predictive control for load shaping and voltage control in smart grids," *IEEE Transactions on Smart Grid*, vol. 10, no. 3, pp. 2334–2344, 2019.

[13] M. Farivar and S. H. Low, "Branch flow model: Relaxations and convexification—part I," *IEEE Transactions on Power Systems*, vol. 28, no. 3, pp. 2554–2564, 2013.

[14] S. Wang, S. Chen, L. Ge, and L. Wu, "Distributed generation hosting capacity evaluation for distribution systems considering the robust optimal operation of OLTC and SVC," *IEEE Transactions on Sustainable Energy*, vol. 7, no. 3, pp. 1111–1123, 2016.

[15] N. Jayasekara, M. A. S. Masoum, and P. J. Wolfs, "Optimal operation of distributed energy storage systems to improve distribution network load and generation hosting capability," *IEEE Transactions on Sustainable Energy*, vol. 7, no. 1, pp. 250–261, 2016.

[16] K. Baker, A. Bernstein, E. Dall'Anese, and C. Zhao, "Network-cognizant voltage droop control for distribution grids," *IEEE Transactions on Power Systems*, vol. 33, no. 2, pp. 2098–2108, 2018.

[17] C. Spanias, P. Aristidou, and M. Michaelides, "Demand-side volt/var/watt regulation for effective voltage control in distribution grids," in *Proc. IEEE PES Innovative Smart Grid Technologies Europe (ISGT-Europe)*, 2019, pp. 1–5.

[18] Y. Guo, X. Zhou, C. Zhao, Y. Chen, T. Summers, and L. Chen, "Solving optimal power flow for distribution networks with state estimation feedback," in *Proc. American Control Conference*, 2020, pp. 3148–3155.

[19] M. Picallo, S. Bolognani, and F. Dörfler, "Closing the loop: Dynamic state estimation and feedback optimization of power grids," *Electric Power Systems Research*, vol. 189, p. 106753, 2020.

[20] Y. R. Rodrigues, M. M. A. Abdelaziz, and L. Wang, "D-PMU based distributed voltage and frequency control for DERs in islanded microgrids," *IEEE Transactions on Sustainable Energy*, vol. 12, no. 1, pp. 451–468, 2021.

[21] M. Almassalkhi *et al.*, *Asynchronous Coordination of Distributed Energy Resources with Packetized Energy Management*. New York, NY: Springer New York, 2018, pp. 333–361.

[22] M. Almassalkhi, J. Frolik, and P. Hines, "Packetized energy management: Asynchronous and anonymous coordination of thermostatically controlled loads," in *Proc. American Control Conference (ACC)*, May 2017, pp. 1431–1437.

[23] L. A. D. Espinosa, M. Almassalkhi, P. Hines, and J. Frolik, "Aggregate modeling and coordination of diverse energy resources under packetized energy management," in *Proc. IEEE 56th Annual Conference on Decision and Control (CDC)*, Dec 2017, pp. 1394–1400.

[24] L. A. D. Espinosa, A. Khurram, and M. Almassalkhi, "Reference-tracking control policies for packetized coordination of heterogeneous der populations," *IEEE Transactions on Control Systems Technology*, pp. 1–17, 2020.

[25] L. A. Duffaut Espinosa and M. Almassalkhi, "A packetized energy management macromodel with quality of service guarantees for demand-side resources," *IEEE Transactions on Power Systems*, vol. 35, no. 5, pp. 3660–3670, 2020.

[26] L. A. D. Espinosa, A. Khurram, and M. R. Almassalkhi, "A virtual battery model for packetized energy management," in *Proc. 59th IEEE Conference on Decision and Control (CDC)*, 2020, pp. 42–48.

[27] A. Khurram, L. A. D. Espinosa, and M. R. Almassalkhi, "A methodology for quantifying flexibility in a fleet of diverse ders," in *Proc. IEEE PowerTech*, 2021, pp. 1–6.

[28] S. Brahma, A. Khurram, H. Ossareh, and M. Almassalkhi, "Optimal frequency regulation using packetized energy management," 2021, Under review at: https://arxiv.org/abs/2107.12939.

[29] A. Inaolaji, A. Savasci, S. Paudyal, and S. Kamalasadan, "Accuracy of phase-decoupled and phase-coupled distribution grid power flow models," in *Proc. IEEE Power Energy Society Innovative Smart Grid Technologies Conference (ISGT)*, 2021, pp. 1–5.

[30] V. Kekatos, L. Zhang, G. B. Giannakis, and R. Baldick, "Voltage regulation algorithms for multiphase power distribution grids," *IEEE Transactions on Power Systems*, vol. 31, no. 5, pp. 3913–3923, 2016.

[31] K. P. Schneider, B. A. Mather, B. C. Pal, C.-W. Ten, G. J. Shirek, H. Zhu, J. C. Fuller, J. L. R. Pereira, L. F. Ochoa, L. R. de Araujo, R. C. Dugan, S. Matthias, S. Paudyal, T. E. McDermott, and W. Kersting, "Analytic considerations and design basis for the ieee distribution test feeders," *IEEE Transactions on Power Systems*, vol. 33, no. 3, pp. 3181–3188, 2018.

[32] N. Li, G. Qu, and M. Dahleh, "Real-time decentralized voltage control in distribution networks," in *Proc. 52nd Annual Allerton Conference on Communication, Control, and Computing (Allerton)*, 2014, pp. 582–588.